Hindawi
Advances in Mathematical Physics
Volume 2022, Article ID 2224435, 18 pages
https://doi.org/10.1155/2022/2224435

Research Article

Radiative and MHD Effects on Time-Dependent Thermal-Material Transfer by Micropolar Binary Mixture

Md. Mosharrof Hossain,[1] **R. Nasrin**,[1] **and Md. Hasanuzzaman**[2]

[1]*Department of Mathematics, Bangladesh University of Engineering and Technology, Dhaka 1000, Bangladesh*
[2]*Department of Mathematics, Khulna University of Engineering and Technology, Khulna 9203, Bangladesh*

Correspondence should be addressed to R. Nasrin; rehena@math.buet.ac.bd

Received 10 August 2022; Revised 13 October 2022; Accepted 19 October 2022; Published 10 November 2022

Academic Editor: Ghulam Rasool

Radiation is an important branch of thermal engineering which includes geophysical thermal insulation, ground water pollution, food processing, cooling of electronic components, oil recovery processes etc. An analysis of unsteady magneto-convective heat-mass transport by micropolar binary mixture of fluid passing a continuous permeable surface with thermal radiation effect has been introduced in this paper. The governing equations are transformed into coupled ordinary differential equations along with Boussinesq approximation by imposing the similarity analysis. Applying the shooting technique, the obtained non-linear coupled similarity equations are solved numerically with the help of "ODE45 MATLAB" software. The results of the numerical solutions to the problem involving velocity, temperature, concentration and micro-rotation are presented graphically for different dimensionless parameters and numbers encountered. With an increase of suction parameter, the velocity distributions very closed to the inclined permeable wall decrease slightly where $0 \le \eta \le 0.3$. But for the uplifting values of sunction, both micro-rotation profile and species concentration enhance through the boundary layer. The skin-friction coefficient increases about 61%, 13%, 27% for rising values of Prandtl number (0.71-7), radiation effect (0 - 1) and thermal Grashof number (5-10), respectively, but an adverse effect is observed for magnetic field (1 - 4), inclined angle $(0^0 - 60^0)$ and Schmidt number (0.22 - 0.75). Heat transfer and mass transfer reduce about 82%, 53%, respectively, in increasing of *Pr* (0.71-1) and 36%, 11%, respectively, in increasing of thermal radiation (0 - 1). The surface couple stress increases about 26%, 49%, 64% and 30% with the increasing values of magnetic field (1-4), inclination angle $(0^0 - 60^0)$, suction (0-1) and Schmidt number (0.22-0.75), respectively. Finally, the present study has been compared with the earlier published results. It is observed that the comparison bears a good agreement.

1. Introduction

Some non-Newtonian fluids are common to flow along a vertical surface in industrial engineering processes. These non-Newtonian fluids include molten polymers, fossil fuels, animal blood, pulps and fluids which contain certain additives, etc. which are occasionally available in industrial production. Earlier the researchers of fluid dynamics have played a great role in explaining the flow of these non-Newtonian fluids through the stretching surfaces in vertical as well as horizontal positions. In the case of continuous moving surfaces, many practical applications of boundary layer flow are remarkable in industrial and engineering processes. The boundary layer along a liquid film in condensation processes, crystal growth, the moving of heat-treated material between feed and wind-up rolls, aerodynamic extrusion of plastic sheets, many metallurgical processes, such as drawing of continuous filaments through steady fluids, cooling of an infinite metallic plate in a cooling path, which may be an electrolyte, etc., are some notable examples of such continuous moving surfaces. The properties of steady natural convective fluid flow, heat and mass transfer passing an isothermal vertical surface embedded in a permeable medium were predicted by the non-Newtonian fluid flow model [1–4]. Considering heat absorption in a permeable medium, the effects of chemical reaction were discussed

by Rao et al. [5]. Additionally, they studied the effects of a semi-infinite vertical surface on an unstable magnetohydrodynamic free convection fluid flow. Ali et al. [6] solved the governing equations for an unsteady MHD free convective-viscous fluid flow along an inclined surface taking changeable heat and mass transport. They considered optically thick fluid instead of optically thin and the surface makes a fixed angle with the vertical axis. Implications of variable viscosity and chemical reaction on MHD natural convective radiating flow through an inclined porous plate was investigated by Ali et al. [7]. The MHD flow of a micropolar fluid was studied over a vertical plate with heat generation and suction by Ferdous et al. [8] which leads to look for similarity solutions of the problem by considering the variable wall temperature. In recent time, Arifuzzaman et al. [9] investigated chemically reactive and naturally convective unsteady micropolar fluid flow including nanoparticles passing a vertical permeable surface with mass diffusion, radiation absorption, thermal radiation, heat source and MHD. The familiar boundary layer approximations helped them to develop a flow model.

Magneto-hydrodynamics (MHD) deals with the behavior of fluids which are electrically conducting. It also deals with the properties of magnetism. Some mentionable examples of such magnetofluids are liquid metals, salt water, electrolytes, Plasmas etc. Maxwell's equations of electromagnetism and Navier–Stokes equations of fluid dynamics jointly represent the MHD. Many authors are interested to study MHD for its applications to engineering and geophysics. In presence of suction, Al Mahbub et al. [10] introduced a mathematical model to analyze the theory of micro-rotation of MHD fluids over a stretching plate. Ali et al. [11] found similarity solution of time dependent MHD border layer heat transport and fluid movement over a moving wedge applying the Buongiorno's nanofluid model. The impacts of chemical reaction on the MHD nanofluid over a vertical surface embedded in a permeable medium were presented by Swain et al. [12]. Through the study of Alam and Huda [13], a novel concept was created due to local similarity solutions of an unsteady MHD free convective heat transfer flow. They took into account fluid movement via a porous flat plate without taking internal heat generation into account. In their extension of earlier research, Alam et al. [14] considered the impact of internal heat generation or absorption for free convective heat transfer flow crossing a vertical permeable flat surface.

MHD border layer nanofluid movement and thermal transport through a stretching surface was analyzed by Ali et al. [15]. The effects of chemical reaction on an unsteady MHD free convection fluid flow were demonstrated by Reddy et al. [16]. The flow through a semi-infinite vertical surface embedded in a permeable material with heat absorption was taken into consideration. Thakur and Hazarika [17] showed the influences of thermal conductivity and variable viscosity on unsteady free convective heat - mass transport MHD flow. They considered the micropolar fluid passing a permeable surface in presence constant heat flux. They also considered viscosity and thermal conductivity as the inverse linear functions of temperature. The term "micropolar fluids" refers to complicated fluids having microstructure. The applications of micropolar fluids are extensively found in the field of geophysics, biomechanics, energy systems and industrial engineering etc. In presence of non-uniform heat source and chemical reaction, a numerical study of MHD micropolar fluid was presented by [18–20] along a stretching sheet embedded in permeable surface. Applying micropolar fluids model and hydrodynamic characteristics with default function in FLUENT was analyzed by Wang et al. [21]. Considering the heat transfer by radiative influence, Baruah and Hazarika [22] discussed the impacts of variable viscosity as well as thermal conductivity on unsteady micropolar fluid around a porous cylinder. Haque [23] deeply studied the impacts of induced magnetic field on the transient heat-mass transport and MHD micropolar fluid flow. He thought of fluid flow crossing a vertical surface that is semi-infinite and surrounded by a permeable medium and a steady heat sink.

The migration of tiny particles from a hot surface to a cool one is known as thermophoresis. It plays a great role to micro-particle transport caused by surrounding temperature gradient. The application of thermophoresis is mostly observed in aerosol technology. Darcy mixed convective heat and mass transfer that travel through a permeable wedge along with chemical reaction have been explored previously for the effects of thermophoretic influences. By passing a semi-infinite porous inclined surface with chemical reaction, Mondal et al. [24] observed the Soret-Dufour influences on MHD convective flow. They also observed the effects of thermophoresis in the same environment. Thermal radiation is a process which makes the variation of temperatures in order to exchange energy. Radiation is transmitted from ultraviolet into far-field infrared according as the material temperature. It is an important branch of thermal engineering which includes geophysical thermal insulation, ground water pollution, food processing, cooling of electronic components, oil recovery processes etc. Khader and Megahed [25] presented a numerical simulation applying FDM (Finite Difference Method). They studied the heat transfer and fluid flow along an unsteady stretching sheet embedded in a porous surface. Shamshuddin et al. [26] propagated the research work of Babu et al. [27] in presence of thermal radiation as well as heat source/sink. The consequences of first order chemical reaction and FDM (Finite Difference Method) numerical solutions were also presented for radiative-convection micropolar fluid for an inclined permeable surface. Nazir et al. [28] considered the effects of viscous dissipation, Joule heating, and heat generation on the transport of momentum in a rotating cone under generalized ohm's law and heat. Also, the heat and mass transport past a stretched surface having pores in a pseudo-plastic model were investigated by Wang et al. [29]. They used the MAPLE software in their simulations. Bhatti et al. [30] investigated the electromagnetohydrodynamic (EMHD) dissipative free convection in a micro-channel containing a permeable medium saturated with a viscoelastic fluid. Rasool et al. [31] introduced the concept of entropy optimization in fluid flow through a Darcy channel with a non-linearly stretching surface. Colak et al. [32] demonstrated the efficiency of the ANN procedure

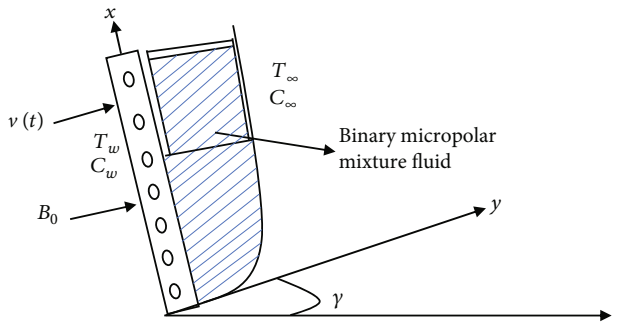

Figure 1: Physical Model and coordinate system.

for Buongiorno's mathematical model using Powell Eyring fluid. This included slip, Darcy-Forchheimer, heat source phenomena, and convective boundary conditions toward a radiative stretching surface.

The innovation of this research work is to explore the thermal radiation effect of unsteady magneto-convective heat and mass transfer by micropolar binary mixture of fluid passing a continuous permeable surface. The main novelty of this research is to compare our numerical results with the published results. We have also enhanced this paper further by considering the induced magnetic force with the inclined angle which has not been explained yet. The current research is to extend the works of Animasaun [33] by considering the effects of the magnetic force parameter and the inclined angle. Three surfaces (horizontal, vertical and inclined surfaces) have been considered to study three positions of the permeable surface at a time to compare the radiative impacts. In this study, we have carefully described the velocity, temperature, concentration and microrotation profiles. The impacts of the thermo-physical parameters on the flow and heat-mass transport characteristics are discussed in detail. Additionally, tabular forms are supplied for the thermophysical parameters of practical importance, including the Nusselt number, Sherwood number, surface couple stress, and coefficient of skin friction.

2. Mathematical Analysis

Figure 1 displays the considered physical geometry. A micropolar binary fluid mixture traveling over a continuous permeable surface is modeled for an unsteady magneto-convective heat-mass transport. The flow is taken into consideration across the x-axis. This is also expected along the semi-infinite surface and y-axis is normal to it. An optically thin fluid is considered with absorption coefficient (α) satisfying the condition $\alpha << 1$. According to Cheng [34], the radiative heat flux $\partial q_r/\partial y$ is approximately represented by the fourth power of temperature in the energy balance equation. The temperature gradient normal to the surface is significantly higher in boundary layer theory than the temperature gradient along the surface, i.e.

$$\frac{\partial \mathrm{T}}{\partial \mathrm{y}} \gg \frac{\partial \mathrm{T}}{\partial \mathrm{x}} \tag{1}$$

For this reason, the thermophoretic velocity component along the surface is ignorable with comparison to velocity component normal to the surface. It is expected that the wall temperature (T_w) is less than the free stream temperature $T_\infty (T_w < T_\infty)$. With the help of Mathematical model presented by Sastry et al. [35], all presumptions expressed above and Boussinesq's approximation; the governing equations can be written as:

$$\frac{\partial v}{\partial y} = 0, \tag{2}$$

$$\frac{\partial u}{\partial t} + v\frac{\partial u}{\partial y} = \left(\frac{\mu + \tau}{\rho}\right)\frac{\partial^2 u}{\partial y^2} + \frac{\tau}{\rho}\frac{\partial N}{\partial y} + g\beta(T - T_\infty)cos\gamma + g\beta^*(C - C_\infty)cos\gamma - \frac{\sigma {B_0}^2}{\rho}u, \tag{3}$$

Here a uniform transverse magnetic field B_0 is set along y-axis i.e., along horizontal direction. Also, the induced magnetic field is ignored which makes magnetic Reynolds as small. Further, there exists no electric field and the Hall effect of MHDs is disregarded.

$$\rho C_p\left(\frac{\partial T}{\partial t} + v\frac{\partial T}{\partial y}\right) = \kappa\frac{\partial^2 T}{\partial y^2} - \frac{\partial q_r}{\partial y} \tag{4}$$

$$\frac{\partial C}{\partial t} + v\frac{\partial C}{\partial y} + \frac{\partial}{\partial y}[V_T(C - C_\infty)] = D_m\frac{\partial^2 C}{\partial y^2}, \tag{5}$$

$$\frac{\partial N}{\partial t} + v\frac{\partial N}{\partial y} + = \frac{\gamma^*}{\rho j}\frac{\partial^2 N}{\partial y^2} - \frac{\tau}{\rho j}\left(2N + \frac{\partial u}{\partial y}\right) \tag{6}$$

Here v can be considered either as a function of time or as constant using continuity equation (2). Makinde [36] has defined the velocity component along y-axis as follows-

$$v = -c\left(\frac{\nu}{t}\right)^{1/2} \tag{7}$$

where $c < 0$ indicates the injection parameter and $c > 0$ represents the suction parameter. Abdel-Rahman [37] and Qasim et al. [38] have introduced micro-inertia per unit mass and spin gradient viscosity as follows:

$$\gamma^* = \left(\mu + \frac{\tau}{2}\right) \text{and } j = \frac{\mu}{\rho U_0} \tag{8}$$

Talbot et al. [39] also introduced the thermophoretic parameter in equation (5) and later by Tsai [40] as-

$$V_T = -\frac{K^{Th}}{T_{ref}} \cdot \frac{\partial T}{\partial y} \tag{9}$$

where K^{Th} represents the thermophoretic coefficient. Batchelor and Shen [41] considered the values of K^{Th} from 0.2 to 1.2. The fluid properties are considered to be same aside

Table 1: Values of skin friction coefficient, heat transfer and mass transfer for Prandtl number variation with $\gamma = 45°$, $M = 2$, $c = 0.5$, $R = 0.5$, $Sc = 0.22$, $L_1 = 0.33$, $\lambda = 1$, $\xi = 3$, $K_1 = 0.5$, $Gr = 10$, $Gc = 10$.

Pr	$f'(0)$	$-\theta'(0)$	$-\varphi'(0)$	$h'(0)$
0.71	3.21254671168802	5.39717494898721	1.61601211434967	0.183990538644394
1.0	4.85182126131598	1.24556598850519	0.814960696921170	-4.52712002627180
7.0	5.18177403861466	0.990889417505988	0.768858246666995	-6.69538231206026

from dynamic viscosity and the effect of density difference with concentration and temperature in the body force term (Boussinesq's approximation).

In 1903, Joseph Boussinesq considered buoyancy-driven flow; he investigated acceleration due to gravity and density differences corresponding to buoyancy driven flow. The density model for slight temperature variation between the wall and free stream layer is given by-

$$\rho = \rho_\infty[1 - \beta(T - T_\infty)] \tag{10}$$

where $g(\rho - \rho_\infty)$ is known as buoyancy term. Applying the above approximation, the buoyancy term is given by-

$$-g\beta\rho_\infty(T - T_\infty) \tag{11}$$

The buoyancy force as well as pressure term is now expressed as $-\partial p/\partial x = g\beta\rho_\infty(T - T_\infty)$. Furthermore, Boussinesq approximation for combined heat and mass transfer convection can be expressed as follows:

$$-\frac{\partial p}{\partial x} = g\beta\rho_\infty(T - T_\infty) + g\beta^*\rho_\infty(C - C_\infty) \tag{12}$$

This principle is known as Boussinesq approximation. According to Boussinesq [42], this approximation indicates the density variation is too small to be ignored.

Then buoyancy model (11) can be modified as-

$$-\frac{\partial p}{\partial x} = g\beta\rho_\infty(T_\infty - T) + g\beta^*\rho_\infty(C_\infty - C) \tag{13}$$

Batchelor [43] has studied the temperature dependent viscosity model and later on it has been accepted by Mukhopadhyay [44]. Animasaun and Anselm [45] have developed $\mu(T) = \mu * [1 + b(T_w - T)]$ which is valid only for $T_w > T_\infty$. This was also changed to the form-

$$\mu(T) = \mu * [1 + b(T_\infty - T)] \tag{14}$$

This satisfies the condition $T_w < T_\infty$

Following Raptis [46], the radiative heat flux q_r is formulated as-

$$q_r = -\frac{4\sigma^*}{3k^*}\cdot\frac{\partial T^4}{\partial y} \tag{15}$$

Here where k^* indicates mean absorption coefficient as well as σ^* represents Stefan-Boltzmann constant. The temperature variations within the flow have been considered as small through the study of Raptis [47]. For this reason, the fluid flow can be written as a linear function of temperature. Neglecting higher order terms in application of Taylor series in T^4 about T_0, we get

$$T^4 \cong 4{T_0}^3T - 3{T_0}^4 \tag{16}$$

Williams Landel-Ferry model, Masuko-Magill model, Arrhenius model, exponential model and Batchelor model are the examples of some models for shear viscosity. The analysts in fluid dynamics are yet practicing on empirical data which reveals the impact of temperature on both vortex and dynamic viscosity of micropolar fluid. Using the relations (13) and (14) in equation (3), we obtain-

$$\frac{\partial u}{\partial t} + \nu\frac{\partial u}{\partial y} = \frac{1}{\rho}\frac{\partial}{\partial y}\left(\mu\frac{\partial u}{\partial y}\right) + \frac{\tau}{\rho}\frac{\partial^2 u}{\partial y^2} + \frac{\tau}{\rho}\frac{\partial N}{\partial y} + g\beta(T_\infty - T)cos\gamma + g\beta^*(C_\infty - C)cos\gamma - \frac{\sigma{B_0}^2}{\rho}u \tag{17}$$

(3) implies that,

$$\rho C_p\left(\frac{\partial T}{\partial t} + \nu\frac{\partial T}{\partial y}\right) = \kappa\frac{\partial^2 T}{\partial y^2} - \frac{\partial q_r}{\partial y} \tag{18}$$

Using the equation (13), the equation (5) becomes-

$$\frac{\partial C}{\partial t} + \nu\frac{\partial C}{\partial y} + \frac{\partial}{\partial y}\left[V_T(C_\infty - C)\right] = D_m\frac{\partial^2 C}{\partial y^2} \tag{19}$$

Using the equation (8), the equation (6) becomes-

$$\frac{\partial N}{\partial t} + \nu\frac{\partial N}{\partial y} = \left[\frac{\mu(T)}{\rho} + \frac{\tau}{2\rho}\right]\frac{\partial^2 N}{\partial y^2} - \frac{\tau U_0}{\mu(T)}\left(2N + \frac{\partial u}{\partial y}\right) \tag{20}$$

Equations (17)–(20) are subjected to the following boundary conditions:

$$u(y,0) = 0\ T(y,0) = T_w\ N(y,0) = 0\ C(y,0) = C_w \text{ for } t \le 0, \tag{21}$$

$$u(0,t) = 0, T(0,t) = T_w, N(0,t) = m_0\frac{\partial u}{\partial t}, C(0,t) = C_w \text{ for } t > 0 \tag{22}$$

$$u(\infty,t) \longrightarrow U_0, T(\infty,t) \longrightarrow T_\infty, N(\infty,t) \longrightarrow 0, C(\infty,t) \longrightarrow C_\infty \text{ for } t > 0 \tag{23}$$

Table 2: Values of skin friction coefficient, heat transfer and mass transfer for thermal Grashof number variation with $\gamma = 45°$, $M = 2$, $c = 0.5$, $R = 0.5$, Pr = 0.71, $Sc = 0.22$, $L_1 = 0.33$, $\lambda = 1$, $\xi = 3$, $K_1 = 0.5$, $Gc = 10$.

Gr	$f'(0)$	$-\theta'(0)$	$-\varphi'(0)$	$h'(0)$
5.0	4.07388893195350	0.990889417505988	0.768858246666995	-5.29972775640911
10.0	5.18177403861466	0.990889417505988	0.768858246666995	-6.69538231206026
20.0	9.61331446048552	0.990889417505988	0.768858246666995	-12.2780005263388
-5.0	-3.68384096734485	0.990889417505988	0.768858246666995	4.96715917106701
-10.0	-4.79172608320034	0.990889417505988	0.768858246666995	6.36281371335391
-15.0	-5.89961117937697	0.990889417505988	0.768858246666995	7.75846828627747

Table 3: Values of skin friction coefficient, heat transfer and mass transfer for radiation parameter variation with $\gamma = 45°$, $M = 2$, $c = 0.5$, Pr = 0.71, Sc = 0.22, $L_1 = 0.33$, $\lambda = 1$, $\xi = 3$, $K_1 = 0.5$, Gr = 10, and Gc = 10.

R	$f'(0)$	$-\theta'(0)$	$-\varphi'(0)$	$h'(0)$
0.0	4.79090445174725	1.29973372953103	0.824898149409840	-4.21723651911105
0.5	5.18177403861466	0.990889417505988	0.768858246666995	-6.69538231206026
1.0	5.43733606529939	0.822078161051940	0.739017613953713	-9.54929448867823
1.5	5.59157104189487	0.713761351236143	0.720266814765392	-13.1670082558130

Table 4: Values of skin friction coefficient, heat transfer and mass transfer for magnetic variation with $\gamma = 45°$, $c = 0.5$, Pr = 0.71, Sc = 0.22, $L_1 = 0.33$, $\lambda = 1$, $\xi = 3$, $K_1 = 0.5$, Gr = 10, and Gc = 10.

M	$f'(0)$	$-\theta'(0)$	$-\varphi'(0)$	$h'(0)$
1.0	5.72444236952871	0.990889417505988	0.768858246666995	-7.59438116227372
2.0	5.18177403861466	0.990889417505988	0.768858246666995	-6.69538231206026
3.0	4.79224467399571	0.990889417505988	0.768858246666995	-6.05963851875451
4.0	4.49557675268770	0.990889417505988	0.768858246666995	-5.58253966814988

Table 5: Values of skin friction coefficient, heat transfer and mass transfer for inclined angle variation with $M = 2$, $c = 0.5$, $Pr = 0.71$, $Sc = 0.22$, $L_1 = 0.33$, $\lambda = 1$, $\xi = 3$, $K_1 = 0.5$, $Gr = 10$, $Gc = 10$.

γ	$f'(0)$	$-\theta'(0)$	$-\varphi'(0)$	$h'(0)$
0	7.24736133524225	0.990889417522182	0.768858246652964	-9.39983346267631
15	7.00758186762903	0.990889417522182	0.768858246480935	-9.08589281897296
30	6.30234813000063	0.990889417522182	0.768858246636872	-8.16253787369599
45	5.18173172460182	0.990889417522182	0.768858246661996	-6.69532691072302
60	3.72119265877469	0.990889417522182	0.768858246688495	-4.78305887759107

Table 6: Values of skin friction coefficient, heat transfer and mass transfer for suction variation with $\gamma = 45°$, $M = 2$, Pr = 0.71, $Sc = 0.22$, $L_1 = 0.33$, $\lambda = 1$, $\xi = 3$, $K_1 = 0.5$, $Gr = 10$, $Gc = 10$.

c	$f'(0)$	$-\theta'(0)$	$-\varphi'(0)$	$h'(0)$
0.0	5.10393225663693	0.754015709395395	0.726018289478001	-10.9968056333437
0.5	5.18173172460182	0.990889417522182	0.768858246661996	-6.69532691072302
1.0	5.17570295073676	1.31709540326671	0.829053291533171	-4.00154822486430
2.0	5.17555633186670	2.03718619317759	0.964865407683984	-1.05227952420773

The above boundary conditions are valid when $T_w < T_\infty$ and $C_w < C_\infty$. In Equation (22) when $m_0 = 0$, we have $N(0, t) = 0$ which indicates no-spin condition. This means that the microelements in a concentrated substance of the fluid adjacent to the wall as if flows cannot spin.

We introduce the following dimensionless vinary differential equations as foll-(19):

$$\eta = \frac{y}{2\sqrt{\nu t}}; f(\eta) = \frac{u}{U_0}; \theta = \frac{T}{T_\infty}; \varphi = \frac{C}{C_\infty}; N = \frac{U_0}{\sqrt{\nu t}} h(\eta) \quad (24)$$

Table 7: Values proportional to the skin friction coefficient, heat transfer and mass transfer for Schmidt number variation with $\gamma = 45°$, $M = 2$, $c = 0.5$, $P_r = 0.71$, $L_1 = 0.33$, $\lambda = 1$, $\xi = 3$, $K_1 = 0.5$, $Gr = 10$, $Gc = 10$.

Sc	$f'(0)$	$-\theta'(0)$	$-\varphi'(0)$	$h'(0)$
0.22	5.18173172460182	0.990889417522182	0.768858246661996	-6.69532691072302
0.60	4.13692092049024	0.990889417522182	1.59539377993130	-4.99847576418460
0.75	3.93292612255038	0.990889417522182	1.89753176459948	-4.69316296608705

Table 8: Comparison of local heat transfer rate $-\theta'(0)$ for thermal radiation parameter (R) applying Classical Runge–Kutta along with shooting technique Animasaun [33] and shooting technique through "ODE45 MATLAB".

R	$-\theta'(0)$ [Animasaun [33]]	$-\theta'(0)$ [present study]	Percentage of error
0.2	-0.918684199255	-0.890007706418090	0.02867649283691
0.4	-0.828710139234	-0.799137657445686	0.02957248178831

Table 9: Comparison of local mass transfer rate $-\varphi'(0)$ for Schmidt number (Sc) applying Classical Runge–Kutta along with shooting technique Animasaun [33] and shooting technique through "ODE45 MATLAB".

Sc	c	$-\varphi'(0)$[Animasaun [33]]	$-\varphi'(0)$ [present study]	Percentage of error
0.22	0.0	-0.582727235867182	-0.590842078810744	0.008114842943562
0.42	0.0	-0.860039307005880	-0.870115821679177	0.010076514673297
0.62	0.0	-1.099421579293592	-1.10977036325952	0.010348783965928
0.22	0.5	-0.798091264284715	-0.797248614856556	0.000842649428159
0.42	0.5	-1.279330713448670	-1.27276484368469	0.00656586976398
0.62	0.5	-1.728144872634346	-1.71420894149338	0.013935931140966

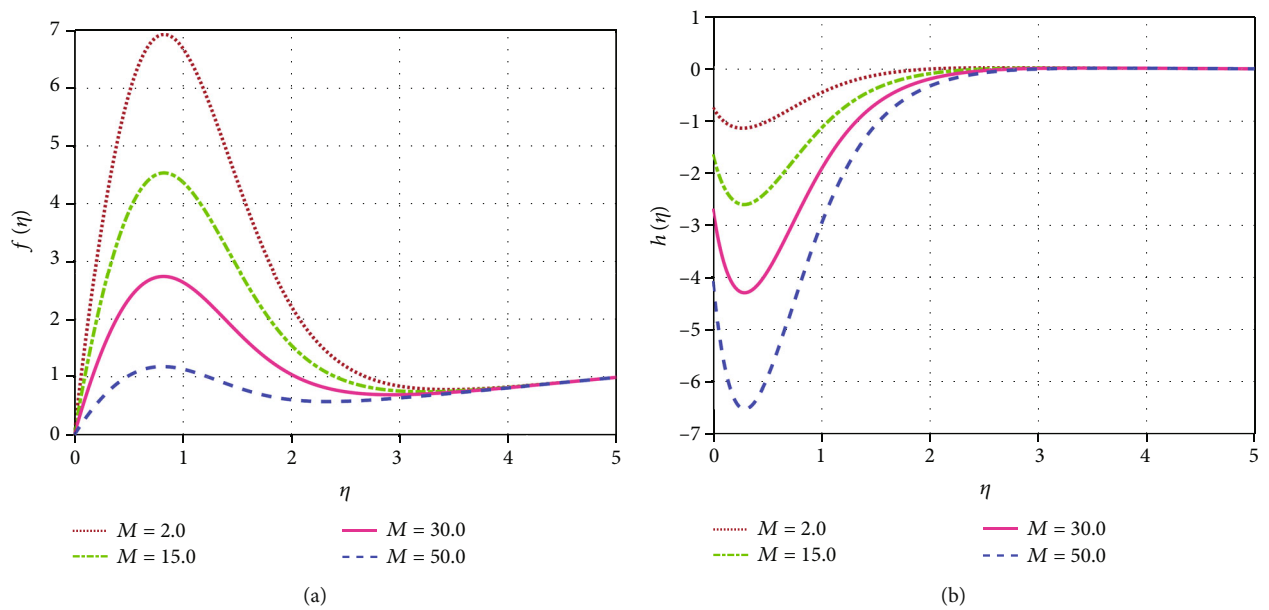

(a) (b)

Figure 2: (a) Velocity, and (b) micro-rotation profiles with constant values of $\gamma = 45°$, $R = 0.5$, $Pr = 0.71$, $Sc = 0.22$, $L_1 = 0.33$, $\lambda = 1$, $\xi = 3$, $K_1 = 0.5$, $Gr = 10$, $Gc = 10$ for magnetic variation.

Finally, we have the dimensionless non-linear ordinary differential equations as follows:

$$(1 + \xi - \theta\xi + k_1)f'' - \xi\theta' f' + 2(\eta + c)f' + 2k_1 h' + G_r\xi(1 - \theta)\cos\gamma + G_c\xi(1 - \varphi)\cos\gamma - Mf = 0 \quad (25)$$

$$\theta'' + \frac{2\Pr}{1 + R}(\eta + c)\theta' = 0, \quad (26)$$

$$\varphi'' + 2S_c(\eta + c)\varphi' - \lambda S_c(1 - \varphi)\theta'' + \lambda S_c\theta'\varphi' = 0 \quad (27)$$

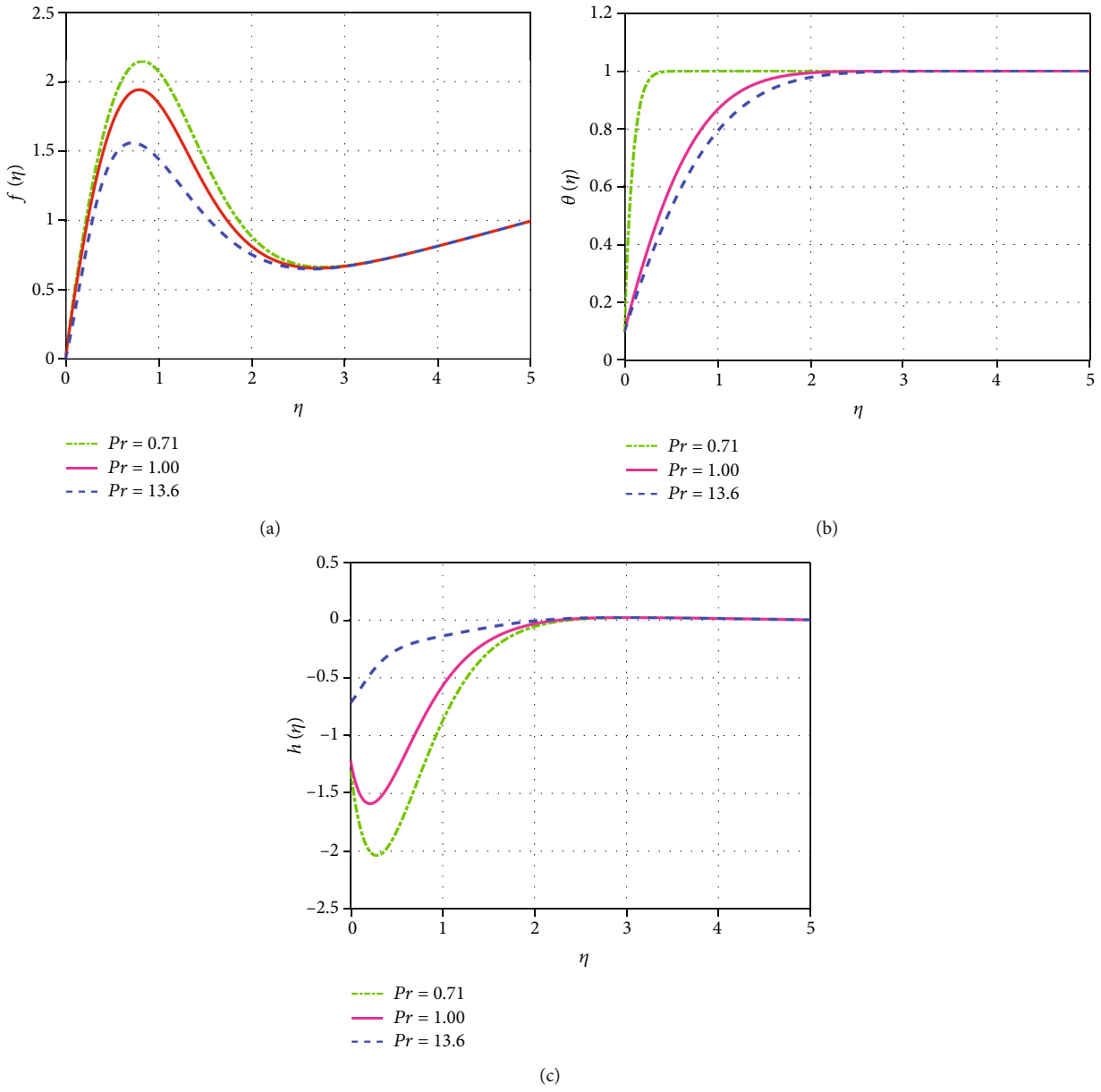

FIGURE 3: (a) Velocity, (b) temperature, and (c) micro-rotation profiles with constant values of $\gamma = 45°$, $M = 2$, $c = 0.5$, $R = 0.5$, $Sc = 0.22$, $L_1 = 0.33$, $\lambda = 1$, $\xi = 3$, $K_1 = 0.5$, $Gr = 10$, $Gc = 10$ for Prandtl number variation.

$$\left(1 + \xi - \theta\xi + \frac{k_1}{2}\right)h'' + 2(\eta + c)h' + 2h - \frac{8L_1}{1 + \xi - \theta\xi}h - \frac{2L_1}{1 + \xi - \theta\xi}f' = 0 \tag{28}$$

Also, the following dimensionless boundary conditions are obtained for the above problem:

$$f(\eta) = 0, \theta(\eta) = \theta_w\,(<1), h(\eta) = -\frac{1}{4}f'(0), \varphi(\eta) = \varphi_w\,(<1) at\ \eta = 0, \tag{29}$$

$$f(\eta) \longrightarrow 1, \theta(\eta) \longrightarrow 1, h(\eta) \longrightarrow 0, \varphi(\eta) \longrightarrow 1 \text{ as } \eta \longrightarrow \infty \tag{30}$$

where $f(\eta)$ is the dimensionless velocity function, $\theta(\eta)$ is the dimensionless temperature function, $\varphi(\eta)$ is the dimensionless concentration function, $h(\eta)$ is the dimensionless micro-rotation function, $Gr = (4tg\beta/U_0 b)$ is the thermal Grashof number, $\xi = bT_\infty$ is the variable viscosity parameter, $k_1 = \tau/\mu$ is the micro-rotation parameter, $Gc = 4tg\beta^*/U_0 b$ is known as the solutal Grashof number, $R = 4t(4\sigma\alpha^2 {T_\infty}^4/\rho C_p T_\infty)$ is the radiation parameter, $\Pr = \nu/\gamma = \mu C_p/\kappa$ is the Prandtl number, $L_1 = k_1 U_0 t$ is defined as the time dependent micro-rotation parameter, $\lambda = -(\kappa^{ThT_\infty}/\nu T_{ref})$ is the thermophoretic parameter, $M = 4\sigma B_0^2 L_1/\rho k_1 U_0$ is the magnetic field parameter, $Sc = \nu/D_m$ is the Schmidt number, γ is the inclined angle of permeable surface with y-axis and η is a similarity variable.

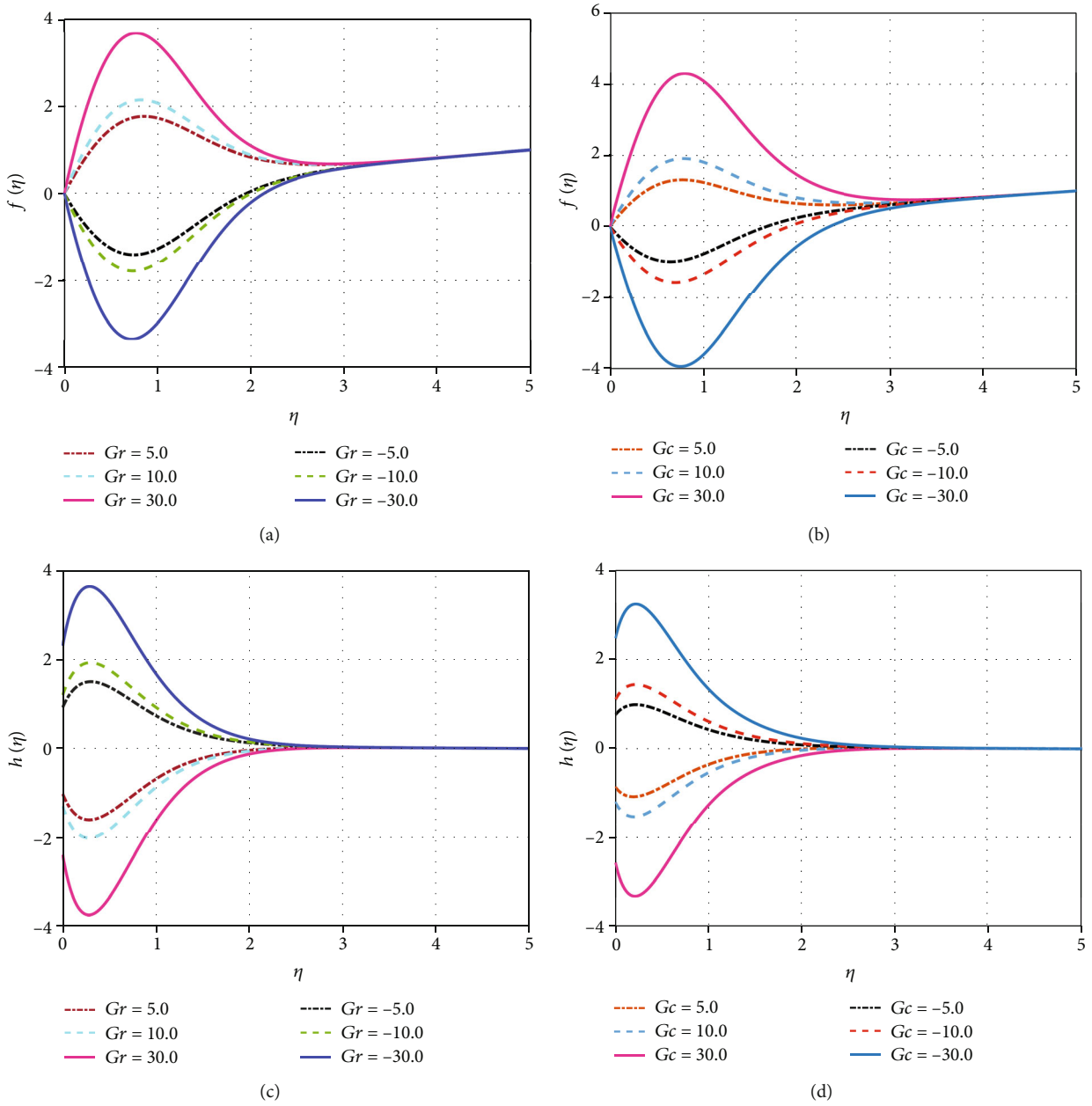

FIGURE 4: Velocity profiles for the variation of (a) thermal Grashof number, (b) solutal Grashof number and micro-rotation profiles for the variation of (c) thermal Grashof number, (d) solutal Grashof number with constant values of $\gamma = 45°$, $M = 2$, $c = 0.5$, $R = 0.5$, $Pr = 0.71$, $Sc = 0.22$, $L_1 = 0.33$, $\lambda = 1$, $\xi = 3$, $K_1 = 0.5$, $Gc = 10$.

3. Numerical Results and Discussion

An analysis of unsteady magneto-convective heat-mass transport by micropolar binary mixture of fluid passing a continuous permeable surface with thermal radiation effect has been introduced in this research work. Firstly, the higher order nonlinear partial differential equations (2)–(6) has been transformed into second order simultaneous linear ordinary differential equations using modified Boussinesq's approximation. Applying the similarity technique, then it has also been converted into initial value problem. Finally, we have solved numerically the coupled non-linear ordinary differential equations (25)–(28) with boundary conditions (29)–(30). Here we have used the shooting technique through "ODE45 MATLAB" software.

Applying the aforesaid numerical procedure, the non-dimensional velocity, temperature, concentration and micro-rotation profiles are determined against the dimensionless coordinate η with the changes of different thermophysical parameters controlling the phenomena of fluid flow. The numerical results are displayed through graphs 2 to 10. The thermo-physical quantities of practical interest such as Nusselt number, coefficient of skin friction and Sherwood number are also calculated and are displayed in Tables 1–7 for analyzing

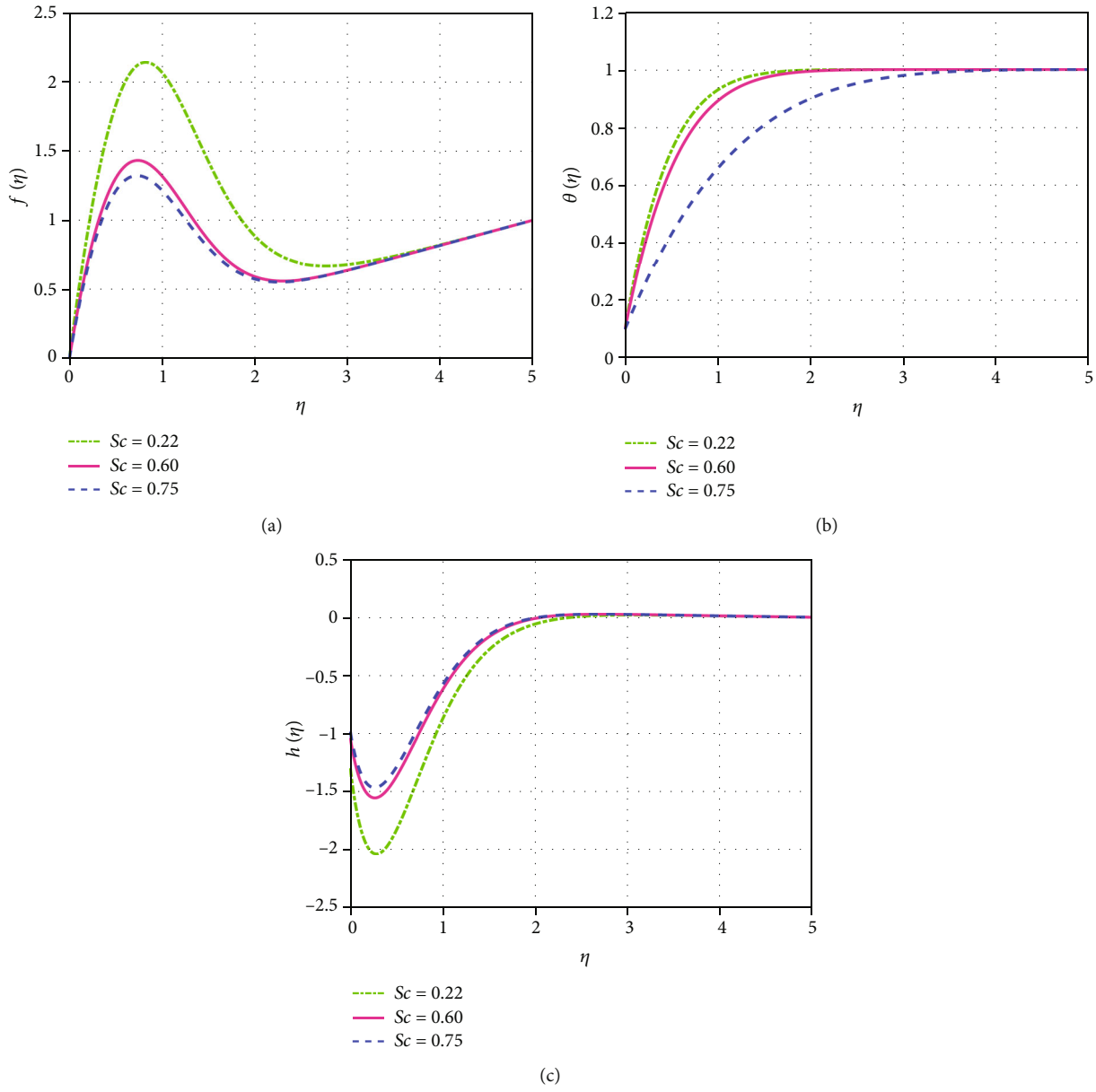

FIGURE 5: (a) Velocity, (b) concentration, and (c) micro-rotation profiles for Schmidt number variation with $\gamma = 45°$, $M = 2$, $c = 0.5$, $R = 0.5$, $Pr = 0.71$, $L_1 = 0.33$, $\lambda = 1$, $\xi = 3$, $K_1 = 0.5$, $Gr = 10$, and $Gc = 10$.

the internal properties of the fluid flow. The comparison between present numerical results and a published paper has been revealed in Tables 8 and 9. We have included here the parameters or numbers as magnetic parameter (M), thermal Grashof number (Gr), Prandtl number (Pr), solutal Grashof number (Gc), Schmidt number (Sc), thermophoretic parameter (λ), thermal radiation parameter (R), micro-rotation parameter (K_1), temperature dependent variable viscosity parameter (ξ), time dependent micro-rotation parameter (L_1), suction parameter (c) and an inclined angle (γ). Here it is noted that we have chosen the changes of some selected numbers or parameters while overlooking the impact of one number or parameter on the field variables. The rest of the numbers or parameters are taken as constants. We have taken the fixed values of parameters or numbers as: $\gamma = 45°$, $Pr = 0.71$, $R = 0.5$, $M = 2$, $c = 0.5$, $L_1 = 0.33$, $\lambda = 1$, $Sc = 0.22$, $\xi = 3$, $K_1 = 0.5$, $Gr = 10$, $Gc = 10$. Furthermore, the boundary conditions have been considered at infinity at a finite point of $\eta = 5$.

3.1. Effect of Magnetic Field. The impacts of magnetic field (M) on fluid velocity and micro-rotation of fluid particles for various values of M have been presented in Figures 2(a) and 2(b). We observe from the figures that the increasing M leads to decrease the velocity fields and also micro-rotation profiles. Because a transversely applied magnetic field generates a Lorentz force. This force acts like a drag force which reduces the fluid motion. Therefore, as the values of M increase, resistive force is also increased resulting a reduction of the velocity and micro-rotation profiles.

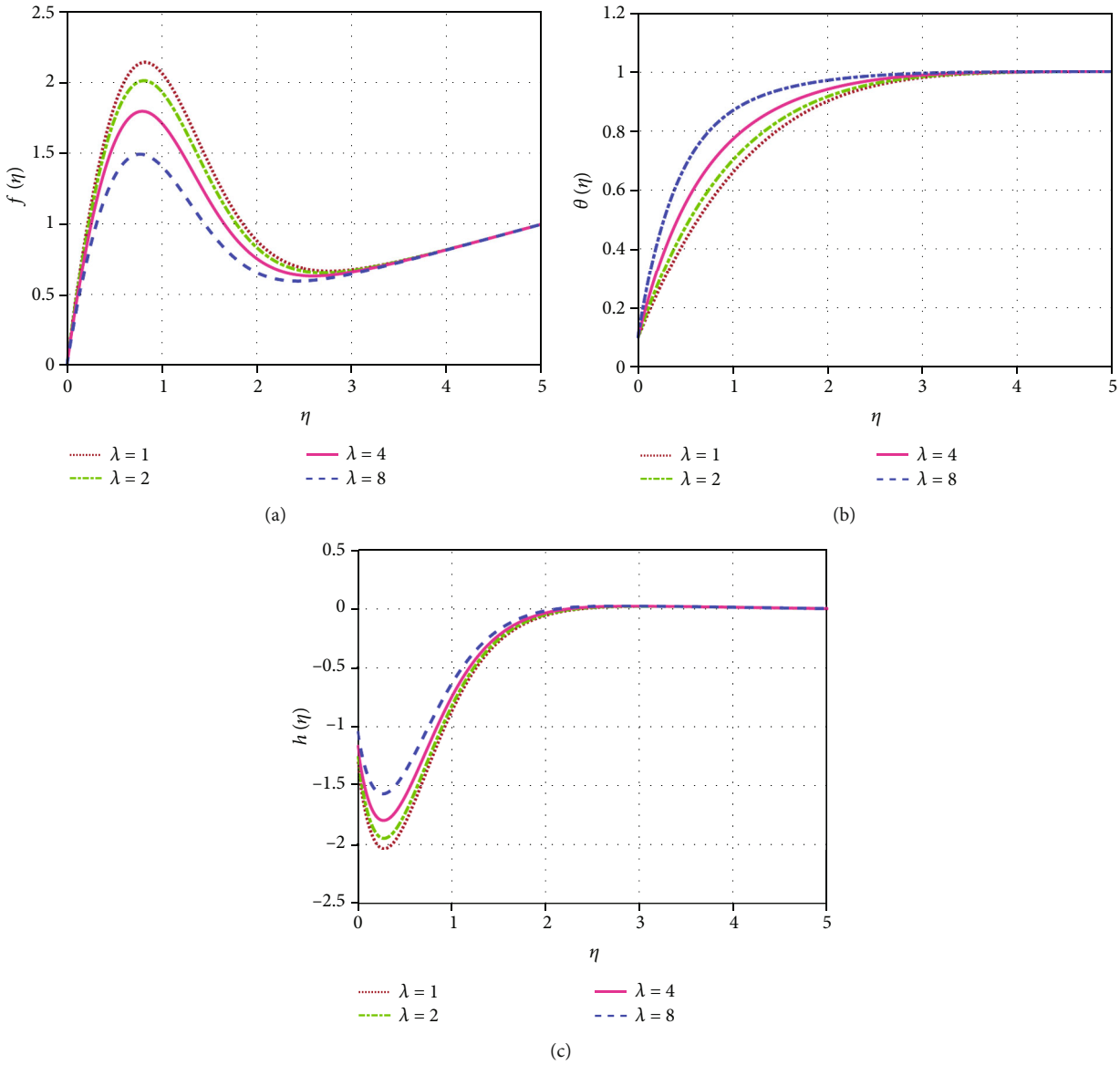

Figure 6: (a) Velocity, (b) concentration, and (c) micro-rotation profiles for thermophoresis variation with $\gamma = 45^{\circ}$, $M = 2$, $c = 0.5$, $R = 0.5$, $Pr = 0.71$, $Sc = 0.22$, $L_1 = 0.33$, $\xi = 3$, $K_1 = 0.5$, $Gr = 10$, and $Gc = 10$.

3.2. Effect of Prandtl Number. The effects of Prandtl number (Pr) on the velocity, temperature and micro-rotation profiles are presented in Figures 3(a)–3(c). The graph 3(a) depicts that with the rising value of Pr, the velocity reduces. Physically, the kinematic viscosity of the fluid promotes owing to increasing values of Prandtl number. This makes the fluid much thicker which reduces the fluid velocity. Figure 3(b) shows that for rising values of Prandtl number, the temperature diminishes. Physically, a higher Prandtl number contains relatively low thermal conductivity. This leads to reduce heat conduction and as a result temperature decreases. Hence for the increasing values of Pr, the rate of heat transfer enhances which reduces the temperature profiles. But an opposite trend is noticed for the micro-rotation profiles with the variation of Prandtl number. The micro-rotation profiles are found to increase noticeably adjacent to the surface $0 \leq \eta \leq 2.2$ and further than its effect is negligible as η increases.

3.3. Effects of Thermal Grashof Number and Solutal Grashof Number. The characteristics of thermal Grashof number and solutal Grashof number on velocity and micro-rotation profiles are presented in Figures 4(a)–4(d). We observed from the Figures 4(a) and 4(b) that the infuences of thermal Grashof number and solutal Grashof number on velocity are identical. For increasing values of Gr and Gc, velocity enhances. But a small variety is noticed for the maximum value of f(η) which are found as 4.25 for Gr and 2.75 for Gc at $\eta = 0.8$. Physically, it is well established that the increase of buoyancy parameters (Gr and Gc) enhances the fluid flow. It is also seen from both the figures that thermal Grashof number and solutal Grashof number have no

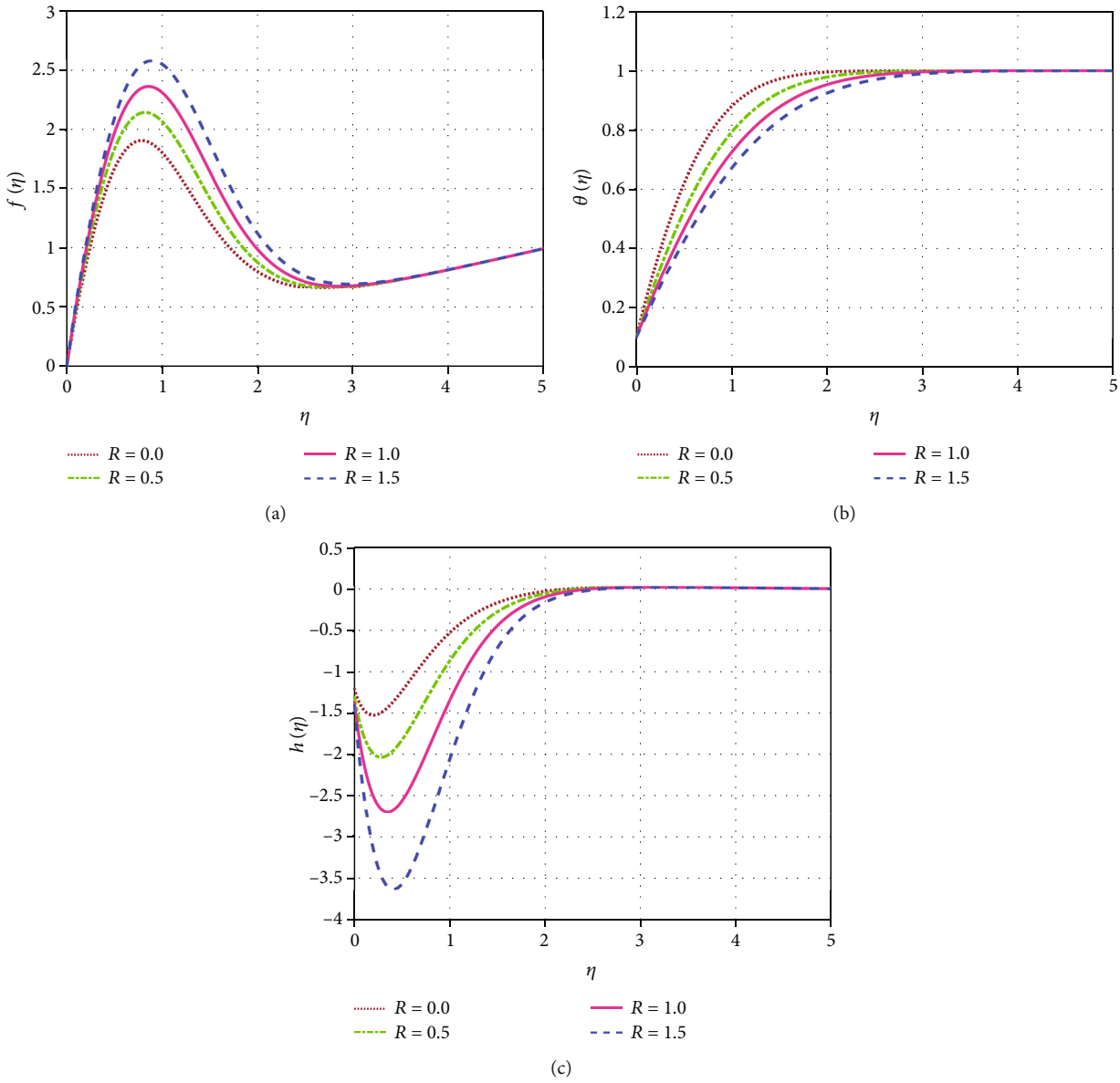

Figure 7: (a) Velocity, (b) concentration, and (c) micro-rotation profiles for thermal radiation variation with $\gamma = 45°$, $M = 2$, $c = 0.5$, $Pr = 0.71$, $Sc = 0.22$, $L_1 = 0.33$, $\lambda = 1$, $\xi = 3$, $K_1 = 0.5$, $Gr = 10$, and $Gc = 10$.

influence as the fluid move away from the bounding surface where $3.2 \leq \eta \leq 5$.

The impacts of local thermal and solutal Grashof number on the microrotation distributions are found same in Figures 4(c) and 4(d). As they increase from zero to positive values, the microrotation of the fluid particles decreases from negative side near the wall in the region $0 \leq \eta \leq 2.4$. Thereafter, there is no influence of Gr and Gc on the microrotation of fluid particles and finally, asymptotically approach 0 as $\eta \to 5$. Hence the micro-rotation profiles are highly influenced by fluids within the domain. The behaviors of local thermal and solutal Grashof number on the microrotation distributions are found same in Figures 4(c) and 4(d). As they increase from zero to positive values, the microrotation of the fluid particles decreases from negative side near the wall in the region $0 \leq \eta \leq 2.4$. Thereafter, there is no influence of Gr and Gc on the microrotation of fluid particles and finally, asymptotically approach 0 as $\eta \to 5$.

3.4. Effect of Schmidt Number. Figures 5(a)–5(c) describe the velocity, concentration and micro-rotation profiles for several values of the Schmidt number. It is observed from the Figures 5(a)–5(b) that velocity and concentration reduce with an increase of Sc value. Since Sc defines the ratio of kinematic viscosity (momentum diffusivity) with the diffusivity of the particle (mass diffusivity), so an increase of Sc corresponds to a reduction of mass diffusivity where the viscosity of the medium enhances and consequently, the velocity of the fluid is reduced. From the figure it is seen that for increasing values of Sc, concentration boundary layer becomes thinner. This leads to reduce the concentration profiles. In a physical manner, molecular diffusivity decreases

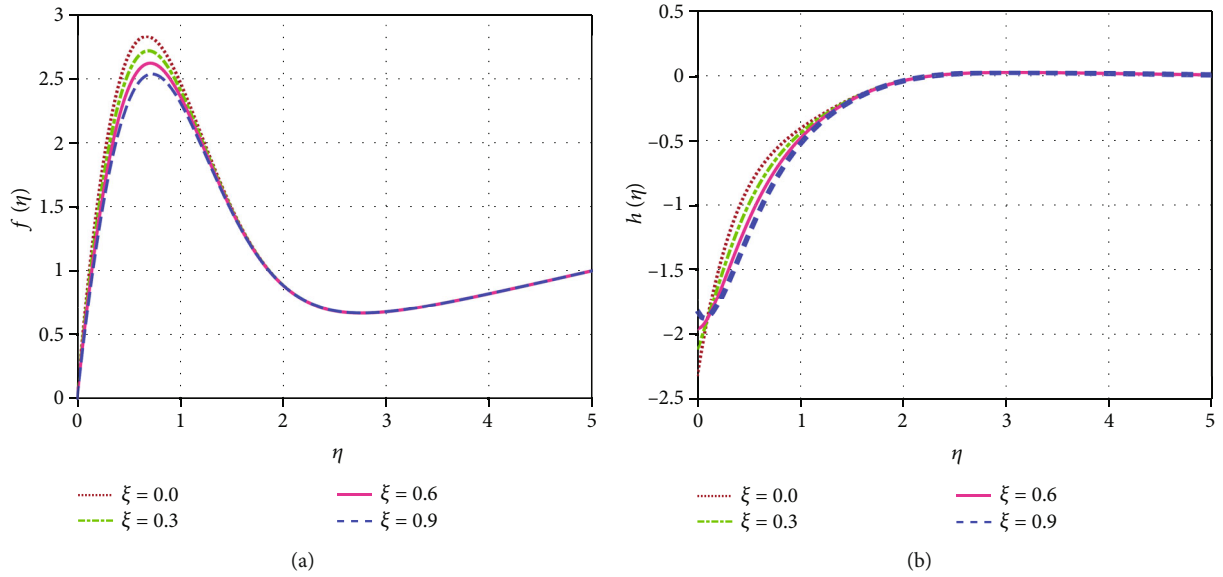

FIGURE 8: (a) Velocity, and (b) micro-rotation profiles for viscosity variation with $\gamma = 45°$, $M = 2$, $c = 0.5$, $R = 0.5$, $Pr = 0.71$, $Sc = 0.22$, $L_1 = 0.33$, $\lambda = 1$, $K_1 = 0.5$, $Gr = 10$, and $Gc = 10$.

due to an increase in magnitude of *Sc*. For that reason, the species concentration is lower for large values of Schmidt number and higher for small values of the Schmidt number. Figure 5(c) is sketched to observe the effects of Schmidt number (*Sc*) on the micro-rotation profiles. The higher value of *Sc* corresponds to a big increase of the micro-rotation profiles in a closed proximity to the wall $0 \le \eta \le 2.2$ and thereafter no change of the behavior is seen and finally approach zero asymptotically all together.

3.5. Effect of Thermophoresis. Figures 6(a)–6(c) illustrate the velocity, concentration, and micro-rotation profiles for various values of thermophoretic parameter (λ). Since the increasing value of thermophoretic parameter reduces the momentum boundary layer thickness and hence the velocity diminishes. An opposite behavior is observed for concentration and micro-rotation of the fluid particles as λ increases. The fluid velocity increases rapidly due to a small change in the thermophoresis parameter. This creates overplus heat energy which leads to rapid increase in the concentration distribution. We also overlooked that an enhancement in the thermophoretic parameter holds relatively large impacts on the micro-rotation of fluid particles adjacent to the wall ($0 \le \eta \le 2.2$). After that, like *Sc* the micro-rotation profiles have no effect and tend to zero asymptotically when $\eta \to 5$.

3.6. Effect of Thermal Radiation. Figures 7(a)–7(c) describe the impact of thermal radiation parameter (R) on the velocity, temperature, and micro-rotation profiles. Since the radiation parameter is the ratio of conduction heat transfer and thermal radiation transfer, rising values of R enhance temperature. As a result, fluid viscosity decreases and velocity upturns within the boundary layer.

Contrary, the thermal boundary layer always found to thicken in presence of radiation, since radiation gives an additional means to disseminate energy. Consequently, the temperature lessens with increasing values of radiation parameter (R). We also noticed that temperature increases for uplifting values of η with radiation parameter. In the range of $0 \le \eta \le 2.6$, the micro-rotation profiles decrease with increasing R and after that no effect is observed with increasing η and asymptotically approaches zero as $\eta \to 5$.

3.7. Effect of Variable Viscosity. Figures 8(a) and 8(b) display the velocity and micro-rotation profiles for several values of temperature dependent variable viscosity parameter (ξ). As ξ enhances, the velocity profiles very close to the wall are negligible where $0 \le \eta \le 0.3$ and thereafter tend to decrease ($0.3 \le \eta \le 1.2$) and finally approach 1 asymptotically as $\eta \to 5$. From Figure 8(b), it is obvious that the micro-rotation of the fluid particles rises averagely with the uplifting value of ξ, very near to the wall $0 \le \eta \le 0.1$; but an alternate behavior is observed when $0.1 \le \eta \le 1.4$ thereafter. Here the micro-rotation profiles diminish slightly with the upturning value of ξ and lead to zero asymptotically as $\eta \to 5$.

3.8. Effect of Suction. From Figures 9(a)–9(c), we observed the impacts of suction parameter (c) on the velocity of the fluids, the chemical species concentration and micro-rotation field. As we expect, if the temperature at the free stream is less than the wall temperature, then rising values of suction parameter (c) correspond to a reduction of fluid velocity from the wall to the free stream (for the case of cooling of the surface, i.e. for $Gr > 0$). This is because of suction removes the low momentum fluid around the heated wall. For this reason, both separation and transition are delayed. Since the fluid adjacent to the heated wall ($\eta = 0$) is pushed towards the region where the buoyancy forces reduce the fluid motion owing to the large effect of viscosity. We also observed that with an enhancement of suction ($c > 0$), the

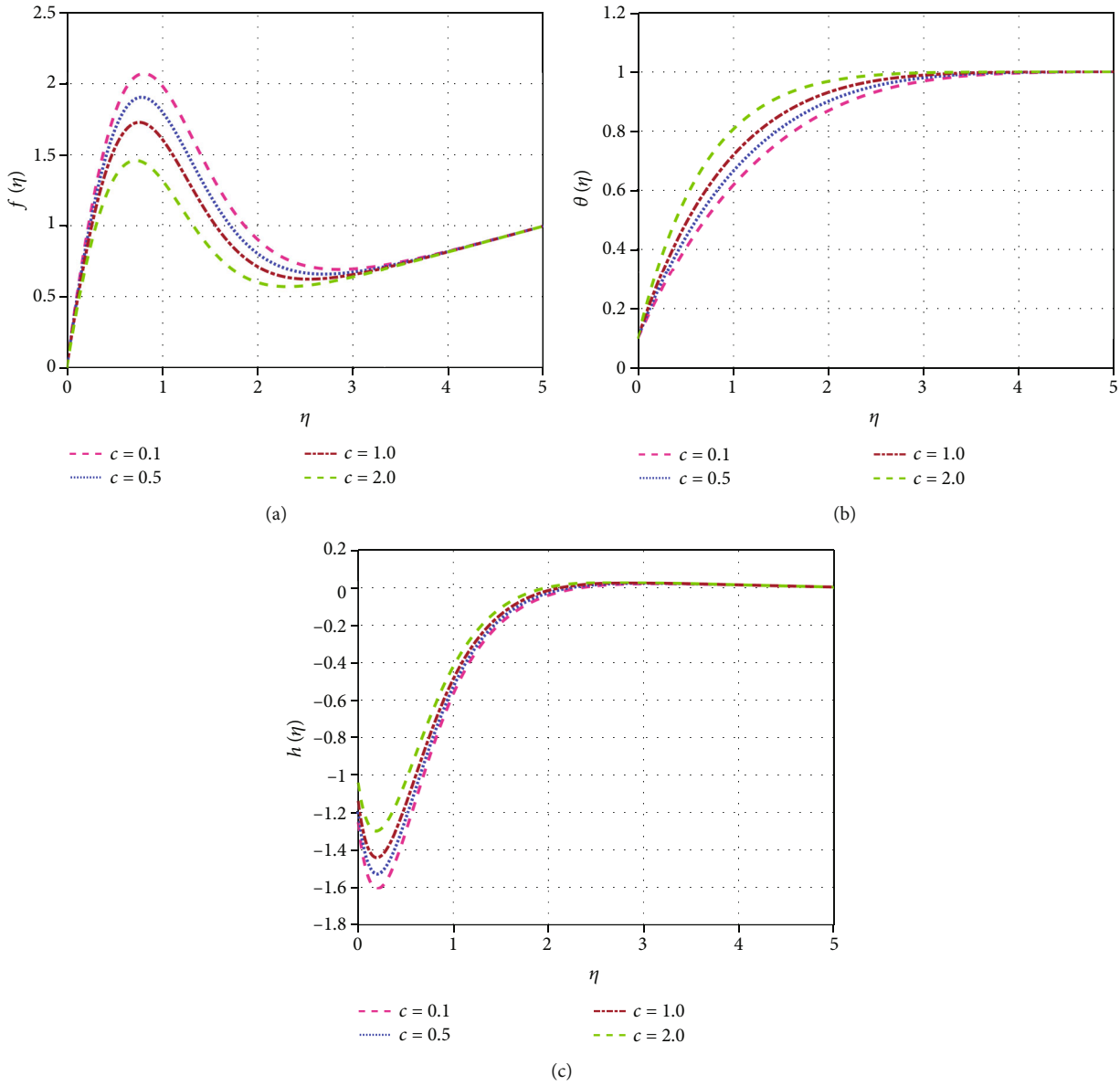

FIGURE 9: (a) Velocity, (b) concentration, and (c) micro-rotation profiles for suction variation with $\gamma = 45°$, $M = 2$, $R = 0.5$, $Pr = 0.71$, $Sc = 0.22$, $L_1 = 0.33$, $\lambda = 1$, $\xi = 3$, $K_1 = 0.5$, $Gr = 10$, and $Gc = 10$.

velocity distributions very closed to the inclined permeable wall decreased negligibility where $0 \leq \eta \leq 0.3$. We further noticed that fluid velocity is found to increase with η and are attained to its maximum peak within $0.5 \leq \eta \leq 1.4$ and after that tend to 1 asymptotically as $\eta \to 5$. From the Figure 9(b), it is noticed that an increase in the magnitude of c, the species concentration through the boundary layer also increased. As the species transfer from lower concentration region to the region of higher concentration, increase in suction will remove thin boundary layer passing the inclined permeable surface and as a result, the high dense fluid will concentrate near the surface quickly. We also investigated that the micro-rotation of fluid particles enhances for rising value of c, where $0 \leq \eta \leq 2.6$. Thereafter ($2.6 \leq \eta \leq 5$) the micro-rotation profiles are not influenced with the uplifting value of c.

3.9. Effect of Inclination. Figures 10(a) and 10(b) depict the impact of inclined angle (γ) on the velocity and micro-rotation profiles.

We investigated that the velocity leads to reduce for the uplifting values of inclined angle (γ). For the increasing values of γ, the impact of the buoyancy force reduces due to the multiplication factor $\cos\gamma$ and consequently the velocity decreases rapidly for the increasing value of γ. For horizontal surface ($\gamma = 90^0$), we also see that velocity profile is a strictly monotonic increasing function of η. But an opposed behavior is observed from the Figure 10(b) for

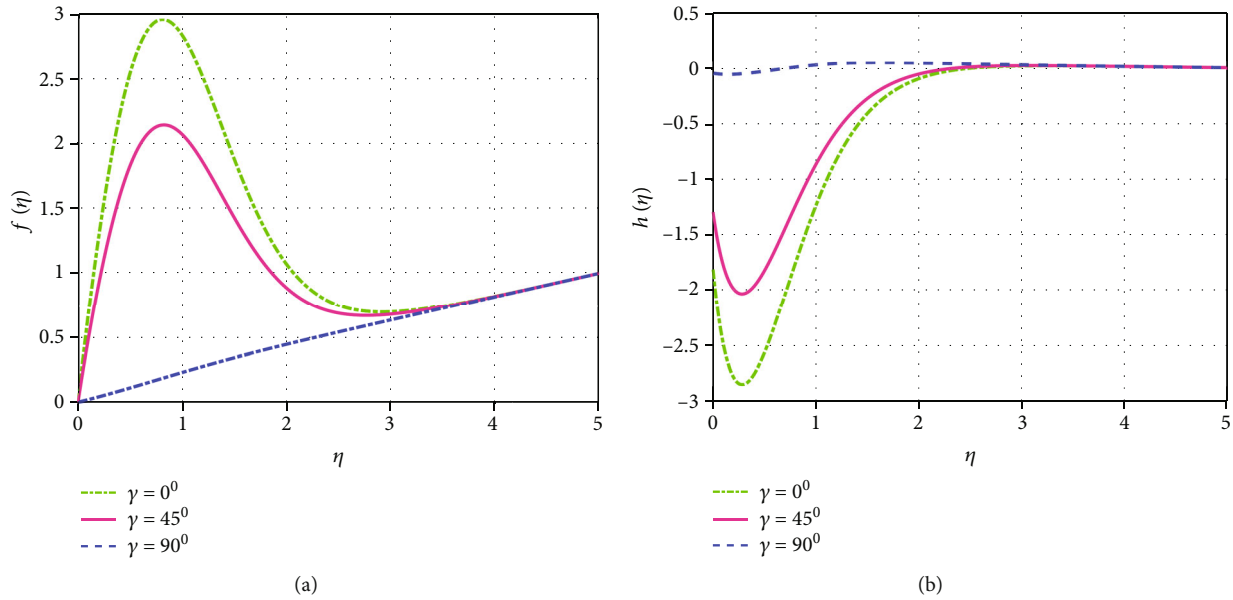

FIGURE 10: (a) Velocity, and (b) micro-rotation profiles for inclined angle variation with $M = 2$, $c = 0.5$, $R = 0.5$, $Pr = 0.71$, $Sc = 0.22$, $L_1 = 0.33$, $\lambda = 1$, $\xi = 3$, $K_1 = 0.5$, $Gr = 10$, and $Gc = 10$.

the increasing values of γ. Because for increasing value of γ, the angular momentum increases within the boundary layer which leads to enhance the micro-rotation profile.

4. Skin Friction, Nusselt Number, Sherwood Number and Surface Couple Stress

The thermo-physical quantities of practical importance such as skin friction coefficient which corresponds to $f'(0)$, Nusselt number (Nu) which corresponds to $\theta'(0)$, Sherwood number (Sh) which corresponds to $\boldsymbol{v}'(0)$ and the surface couple stress $h'(0)$ are also tabulated to explain the internal behavior of the fluid flow:

Table 1 displays how different Prandtl number values affect the types of skin-friction coefficient, Nusselt number, Sherwood number, and surface couple stress. Here, it is noted that only the skin-friction coefficient increases with growing Pr values, whereas all other thermophysical parameters (including the Nusselt number, Sherwood number, and surface couple stress) decrease as Pr values rise. The skin-friction coefficient increases about 61% for uplifting values of the Prandtl number (0.71-7). But Nusselt number, Sherwood number and surface couple stress reduce about 82%, 53% and 3817%, respectively, in increasing of Pr (0.71-1).

Table 2 displays the features of thermal Grashof number (Gr) on skin-friction coefficient, Nusselt number, Sherwood number and. We observe that the coefficient of skin-friction increases in case of mode of cooling ($Gr>0$) and reduces in case of mode of heating ($Gr<0$) but a reverse effect is noticed for the surface couple stress. It is also evident that no effect of Gr is seen on Nusselt number and Sherwood number in both cases ($Gr>0$ and $Gr<0$). It is also revealed that the skin-friction coefficient upturns about 27% whereas the surface couple stress diminishes about 26% with the increasing values of Gr (5-10).

The effects of the radiation parameter (R) on the surface couple stress, Nusselt number, Sherwood number, and skin-friction coefficient are shown in Table 3. Here, it is discovered that only the skin-friction coefficient increases with growing values of R, but all other thermo-physical variables decrease with rising R values. The skin-friction coefficient promotes about 13% for uplifting values of the radiation parameter (0 - 1). But Nusselt number, Sherwood number and the surface couple stress reduces about 36%, 11% and 126%, respectively, in increasing of R (0-1).

Table 4 illustrates how the magnetic parameter (M) affects the skin-friction coefficient, Nusselt number, Sherwood number, and surface couple stress. Here we see that the coefficient of skin-friction reduces for rising values of M but an adverse effect is observed for the surface couple stress. It is also evident that there is no influence of M on Nusselt number and Sherwood number for uplifting values of M. We also reveal that the skin-friction coefficient decreases by about 22% whereas the surface couple stress increases by about 26% with the increasing values of M (1.0-4.0).

The features of the inclined angle (γ) on the surface couple stress, Nusselt number, and Sherwood number are shown in Table 5. We discovered that when values of γ increase, the coefficient of skin-friction decreases, while the surface couple stress has the opposite effect. It is also evident that the upturning values of $\gamma(0^0 - 60^0)$ do not affect the Nusselt number or the Sherwood number. Additionally, we observe that as the values of $\gamma(0^0 - 60^0)$ increase, the skin-friction coefficient decreases by around 49% while the surface couple stress increases by about 49%.

Table 6 details how the suction parameter (c) affects the skin-friction coefficient, Nusselt number, Sherwood number, and surface couple stress. We see that when the values of c

rise, all physical quantities get better. Additionally, we observe that with increasing values of c (0-1), the skin-friction coefficient, Nusselt number, Sherwood number, and surface couple stress all rise by around 2%, 75%, 14%, and 64%, respectively.

The effects of the Schmidt number (Sc) on the skin-friction coefficient, the Nusselt number, the Sherwood number, and the surface couple stress are shown in Table 7. From Table 7, we are clear that the coefficient of skin-friction reduces with an increase in the magnitude of Sc whereas reverse impacts are observed for both Sherwood number and surface couple stress. It is also evident that there is no influence of Sc only on Nusselt number for increasing values of Sc. We also reveal that the skin-friction coefficient decreases by about 24% but the Sherwood number and surface couple stress increase by about 149% and 30%, respectively, with increasing values of Sc (0.22-0.75).

5. Comparison

We have compared the numerical results of the present study with Animasaun [33]. Tables 8 and 9 show the comparison of the Nusselt number for thermal radiation parameter (R) and the Sherwood number for Schmidt number (Sc), respectively, considering present numerical results with mentioned published paper. The current numerical results shown in these Tables 8 and 9 are found to be good in agreement with that of Animasaun [33].

6. Conclusion

The insertion of a continuous permeable surface significantly influences the motion and micro-rotation of the flow field. The fluid velocity enhances within the boundary layer whereas both temperature and micro-rotation of fluid particles reduce for rising values of thermal radiation. The velocity of fluid within the boundary layer increases as the radiation rises, whereas the temperature and the microrotation of fluid particles decrease as the radiation rises. The main findings are as follows:

(i) With the movement of a continuous permeable surface, the velocity decreases, and the angular momentum increases.

(ii) For the increasing value of thermophoretic parameter (λ), the velocity reduces but the species concentration of the fluid and the micro-rotation of particles enhance.

(iii) The micro-rotation of fluid particles increases on average with the increase of ξ, very near to the wall $0 \leq \eta \leq 0.1$. But thereafter, an alternate behavior is observed when $0.1 \leq \eta \leq 1.4$.

(iv) The velocity profile very close to the wall is negligible where $0 \leq \eta \leq 0.3$ and thereafter tends to decrease ($0.3 \leq \eta \leq 1.2$) for increasing value of ξ.

(v) The increase of buoyancy parameters (Gr and Gc) enhances the fluid flow. But the microrotation of the fluid particles decreases significantly from the negative side near the wall in the region $0 \leq \eta \leq 2.4$.

(vi) The velocity and temperature reduction for the rising value of Prandtl number, but the micro-rotation profiles are found to increase significantly adjacent to the surface ($0 \leq \eta \leq 2.2$).

(vii) The velocity and species concentration reduce, and the micro-rotation profiles enhance with the uplifting value of Schmidt number (Sc).

(viii) An increase in radiation parameter (R) leads to an increase in fluid velocity within the boundary layer whereas both temperature and micro-rotation of fluid particles reduce for upturning values of radiation parameter (R).

(ix) With an enhancement of suction parameter ($c > 0$), the velocity distributions very close to the inclined permeable wall decrease slightly where $0 \leq \eta \leq 0.3$. But for the rising values of c, both micro-rotation profile and species concentration enhance through the boundary layer.

(x) Suction parameter, radiation parameter, thermophoretic parameter, Schmidt number, and Prandtl number highly affect the fluid properties.

(xi) The skin friction coefficient enhances but all other thermo-physical quantities reduce with increasing values of both Pr and R.

(xii) In cases of cooling ($Gr > 0$) and heating ($Gr < 0$), the coefficient of skin-friction and the surface couple stress play opposing roles.

(xiii) Only the coefficient of skin-friction reduces for rising values of M but an adverse effect is observed for the surface couple stress.

(xiv) With changes in inclined angle (γ), neither heat transfer nor mass transfer is affected.

(xv) Suction parameter improvements have a positive impact on all physical quantities.

(xvi) The increasing values of the Schmidt number (Sc) result in a drop in the skin-friction coefficient, but an increase in mass transfer and surface couple stress.

Nomenclature

MHD: magneto-hydrodynamics
Sc: Schmidt number
J: density of current
T_∞: free stream temperature
β: volumetric expansion coefficient with temperature
C: fluid concentration, kg m^{-3}
C_∞: free stream concentration
u: velocity component along the x-axis, ms^{-1}
$U_0(t)$: uniform surface velocity

Gr: thermal Grashof number
λ: thermophoretic parameter
τ: vortex viscosity
C_p: specific heat at constant pressure
k_T: thermal diffusion ratio
σ: similarity parameter
g: acceleration due to gravity, ms^{-2}
M: magnetic parameter
ξ: Variable viscosity parameter
τ: local skin friction coefficient
S_h: Sherwood number
θ: dimensionless temperature
q_r: radiative heat flux
R: thermal radiation parameter
c: suction parameter
B: uniform magnetic field, Am^{-1}
φ: dimensionless concentration
T: temperature of fluid, k^{-1}
T_w: wall temperature, k^{-1}
β^*: volumetric expansion coefficient with concentration
ρ: fluid density, kg m^{-3}
C_w: wall concentration, kg m^{-3}
v: velocity component along the y-axis, ms^{-1}
$v(t)$: suction velocity
Gc: solutal Grashof number
C_s: concentration susceptibility
η: similarity variable
T_m: fluid mean temperature
D_m: mass diffusivity coefficient
υ: kinematic viscosity, $m^{-2}s^{-1}$
v_0: suction and blowing
P_r: Prandtl number
t: Time, s
N_u: Nusselt number
f: dimensionless velocity
K': Chemical reaction rate of concentration
κ: thermal conductivity
K_r: chemical reaction parameter
μ: Dynamic viscosity.

Data Availability

The data used to support the findings of this study are available from the corresponding author upon request.

Conflicts of Interest

The author (s) declare (s) that they have no conflicts of interest.

Acknowledgments

The research work is done in the Department of Mathematics, Bangladesh University of Engineering and Technology (BUET), Dhaka, Bangladesh. This article is a part of the first author's PH.D. thesis.

References

[1] H. T. Chen and C. O. K. Chen, "Free convection flow of non-Newtonian fluids along a vertical plate embedded in a porous medium," *Journal of Heat Transfer*, vol. 110, no. 1, pp. 257–260, 1988.

[2] H. Ming-Jer and C. Cha'o-Kuang, "Local similarity solutions of free convective heat transfer from a vertical plate to non-Newtonian power law fluids," *International Journal of Heat and Mass Transfer*, vol. 33, no. 1, pp. 119–125, 1990.

[3] R. Nasrin and M. A. Alim, "Combined effects of viscous dissipation and temperature dependent thermal conductivity on MHD free convection flow with conduction and joule heating along a vertical flat plate," *Journal of Naval Architecture and Marine Engineering*, vol. 6, no. 1, pp. 30–40, 2010.

[4] R. Nasrin and M. A. Alim, "MHD free convection flow along a vertical flat plate with thermal conductivity and viscosity depending on temperature," *Journal of Naval Architecture and Marine Engineering*, vol. 6, no. 2, pp. 72–83, 2010.

[5] A. Rao, S. Sivaiah, and R. S. Raju, "Chemical reaction effects on an unsteady MHD free convection fluid flow past a semi-infinite vertical plate embedded in a porous medium with heat absorption," *Journal of Applied Fluid Mechanics*, vol. 12, no. 3, 2012.

[6] F. Ali, I. Khan, and S. Shafie, "Conjugate effects of heat and mass transfer on MHD free convection flow over an inclined plate embedded in a porous medium," *PLoS One*, vol. 8, no. 6, article e65223, 2013.

[7] M. Ali, M. A. Alim, R. Nasrin, and M. S. Alam, "Study the effect of chemical reaction and variable viscosity on free convection MHD radiating flow over an inclined plate bounded by porous medium," *AIP Conference Proceedings*, vol. 1754, Article ID 040009, 2016.

[8] M. Ferdows and D. Liu, "Natural convective flow of a magneto-micropolar fluid along a vertical plate," *Propulsion and Power Research*, vol. 7, no. 1, pp. 43–51, 2018.

[9] S. M. Arifuzzaman, M. F. U. Mehedi, A. Al-Mamun, P. Biswas, M. K. Islam, and M. Khan, "Magnetohydrodynamic micropolar fluid flow in presence of nanoparticles through porous plate: a numerical study," *International Journal of Heat and Technology*, vol. 36, no. 3, pp. 936–948, 2018.

[10] M. A. Al Mahbub, N. J. Nasu, S. Aktar, and Z. Rahman, "Soret-Dufour effects on the MHD flow and heat transfer of microrotation fluid over a nonlinear stretching plate in the presence of suction," *Applied Mathematics*, vol. 4, no. 6, pp. 864–875, 2013.

[11] M. Ali, M. A. Alim, R. Nasrin, M. S. Alam, and M. J. H. Munshi, "Similarity solution of unsteady MHD boundary layer flow and heat transfer past a moving wedge in a nanofluid using the Buongiorno model," *Procedia Engineering*, vol. 194, pp. 407–413, 2017.

[12] K. Swain, S. K. Parida, G. C. Dash et al., "Chemical reaction effects on MHD slip flow of convective Nanofluid over a vertical plate embedded in porous medium with heat source/sink," *Modelling, Measurement and Control B*, vol. 88, no. 2-4, pp. 1–8, 2019.

[13] M. S. Alam and M. N. Huda, "A new approach for local similarity solutions of an unsteady hydromagnetic free convective heat transfer flow along a permeable flat surface," *International Journal of Advances in Applied Mathematics and Mechanics*, vol. 1, no. 2, pp. 39–52, 2013.

[14] M. S. Alam, M. M. Haque, and M. J. Uddin, "Unsteady MHD free convective heat transfer flow along a vertical porous flat plate with internal heat generation," *International Journal of Advances in Applied Mathematics and Mechanics*, vol. 2, no. 2, pp. 52–61, 2014.

[15] M. Ali, M. A. Alim, R. Nasrin, M. S. Alam, and M. Z. U. Chowdhury, "Magnetohydrodynamic boundary layer nanofluid flow and heat transfer over a stretching surface," *AIP Conference Proceedings*, vol. 1851, Article ID 020022, 2017.

[16] G. R. Reddy, K. R. Sekhar, and A. S. M. Lakshmi, "MHD free convection fluid flow past a semi-infinite vertical porous plate with heat absorption and chemical reaction," *International Journal of Chemical Sciences*, vol. 13, pp. 525–540, 2015.

[17] P. M. Thakur and G. C. Hazarika, "Effects of variable viscosity and thermal conductivity on unsteady free convection heat and mass transfer MHD flow of micropolar fluid with constant heat flux through porous medium," *International Journal of Computer Applications*, vol. 8, pp. 0975–8887, 2015.

[18] R. S. Tripathy, G. C. Dash, S. R. Mishra, and M. M. Hoque, "Numerical analysis of hydromagnetic micropolar fluid along a stretching sheet embedded in porous medium with non-uniform heat source and chemical reaction," *Engineering science and technology, an international journal*, vol. 19, no. 3, pp. 1573–1581, 2016.

[19] M. Ali, M. A. Alim, R. Nasrin, and M. S. Alam, "Numerical analysis of heat and mass transfer along a stretching wedge surface," *Journal of Naval Architecture and Marine Engineering*, vol. 14, no. 2, pp. 135–144, 2017.

[20] M. Ali, R. Nasrin, and M. A. Alim, "Analysis of boundary layer nanofluid flow over a stretching permeable wedge-shaped surface with magnetic effect," *Journal of Naval Architecture and Marine Engineering*, vol. 18, no. 1, pp. 11–24, 2021.

[21] L. Wang, X. Chu, J. Wan, and C. Xiu, "Implementation of micropolar fluids model and hydrodynamic behavior analysis using user-defined function in FLUENT," *Advances in Mechanical Engineering*, vol. 12, no. 7, 2020.

[22] I. Baruah and G. C. Hazarika, "Effects of variable viscosity and thermal conductivity on unsteady micropolar fluid about a permeable cylinder under moving boundaries," *The International Journal of Engineering and Science*, vol. 6, no. 9, pp. 33–41, 2017.

[23] M. M. Haque, "Heat and mass transfer analysis on magneto micropolar fluid flow with heat absorption in induced magnetic field," *Fluids*, vol. 6, no. 3, p. 126, 2021.

[24] H. Mondal, D. Pal, S. Chatterjee, and P. Sibanda, "Thermophoresis and Soret-Dufour on MHD mixed convection mass transfer over an inclined plate with non-uniform heat source/sink and chemical reaction," *Ain Shams Engineering Journal*, vol. 9, no. 4, pp. 2111–2121, 2018.

[25] M. M. Khader and A. M. Megahed, "Numerical simulation using the finite difference method for the flow and heat transfer in a thin liquid film over an unsteady stretching sheet in a saturated porous medium in the presence of thermal radiation," *Journal of King Saud University-Engineering Sciences*, vol. 25, no. 1, pp. 29–34, 2013.

[26] M. D. Shamshuddin, O. Anwar Bég, M. Sunder Ram, and A. Kadir, "Finite element computation of multi-physical micropolar transport phenomena from an inclined moving plate in porous media," *Indian Journal of Physics*, vol. 92, no. 2, pp. 215–230, 2018.

[27] M. S. Babu, J. G. Kumar, and T. S. Reddy, "Mass transfer effects on unsteady MHD convection flow of micropolar fluid past a vertical moving porous plate through porous medium with viscous dissipation," *International Journal of Applied Mathematics and Mechanics*, vol. 9, no. 6, pp. 48–67, 2013.

[28] U. Nazir, M. Sohail, M. M. Selim, H. Alrabaiah, and P. Kumam, "Finite element simulations of hybrid nano-Carreau Yasuda fluid with hall and ion slip forces over rotating heated porous cone," *Scientific Reports*, vol. 11, no. 1, 2021.

[29] F. Wang, U. Nazir, M. Sohail, E. R. El-Zahar, C. Park, and P. Thounthong, "A Galerkin strategy for tri-hybridized mixture in ethylene glycol comprising variable diffusion and thermal conductivity using non-Fourier's theory," *Nanotechnology Reviews*, vol. 11, no. 1, pp. 834–845, 2022.

[30] M. M. Bhatti, O. A. Bég, R. Ellahi, and T. Abbas, "Natural convection non-Newtonian EMHD dissipative flow through a microchannel containing a non-Darcy porous medium: Homotopy perturbation method study," *Qualitative Theory of Dynamical Systems*, vol. 21, no. 4, pp. 1–27, 2022.

[31] G. Rasool, A. Shafiq, I. Khan, D. Baleanu, K. Sooppy Nisar, and G. Shahzadi, "Entropy generation and consequences of MHD in Darcy–Forchheimer nanofluid flow bounded by nonlinearly stretching surface," *Symmetry*, vol. 12, no. 4, p. 652, 2020.

[32] A. B. Çolak, A. Shafiq, and T. N. Sindhu, "Modeling of Darcy-Forchheimer bioconvective Powell Eyring nanofluid with artificial neural network," *Chinese Journal of Physics*, vol. 77, pp. 2435–2453, 2022.

[33] I. L. Animasaun, "Double diffusive unsteady convective micropolar flow past a vertical porous plate moving through binary mixture using modified Boussinesq approximation," *Ain Shams Engineering Journal*, vol. 7, no. 2, pp. 755–765, 2016.

[34] P. Cheng, "Two-dimensional radiating gas flow by a moment method," *American Institute of Aeronautics and Astronautics Journal*, vol. 2, no. 9, pp. 1662–1664, 1964.

[35] D. R. V. S. R. K. Sastry and A. S. N. Murti, "A double diffusive unsteady MHD convective flow past a flat porous plate moving through a binary mixture with suction or injection," *Journal of Fluids*, vol. 2013, Article ID 935156, 10 pages, 2013.

[36] O. D. Makinde, "Free convection flow with thermal radiation and mass transfer past a moving vertical porous plate," *International Communications in Heat and Mass Transfer*, vol. 32, no. 10, pp. 1411–1419, 2005.

[37] G. M. Abdel-Rahman, "Effect of magnetohydrodynamic on thin films of unsteady micropolar fluid through a porous medium," *Journal of Modern Physics*, vol. 2, no. 11, pp. 1290–1304, 2011.

[38] M. Qasim, I. Khan, and S. Shafie, "Heat transfer in a micropolar fluid over a stretching sheet with Newtonian heating," *PLoS One*, vol. 8, no. 4, article e59393, 2013.

[39] M. Z. Haque, M. M. Alam, M. Ferdows, and A. Postelnicu, "Micropolar fluid behaviors on steady MHD free convection and mass transfer flow with constant heat and mass fluxes, joule heating and viscous dissipation," *Journal of King Saud University-Engineering Sciences*, vol. 24, no. 2, pp. 71–84, 2012.

[40] R. Tsai, Y. P. Chang, and T. Y. Lin, "Combined effects of thermophoresis and electrophoresis on particle deposition onto a wafer," *Journal of Aerosol Science*, vol. 29, no. 7, pp. 811–825, 1998.

[41] G. K. Batchelor and C. Shen, "Thermophoretic deposition of particles in gas flowing over cold surfaces," *Journal of Colloid and Interface Science*, vol. 107, no. 1, pp. 21–37, 1985.

[42] J. Boussinesq, "Théorie de l'écoulement tourbillonnant et tumultueux des liquides dans les lits rectilignes a grande section," vol. 1, Gauthier-Villars, 1897.

[43] G. K. Batchelor, *An Introduction to Fluid Dynamics*, Cambridge university press, 2012.

[44] S. Mukhopadhyay, "Effects of radiation and variable fluid viscosity on flow and heat transfer along a symmetric wedge," *Journal of Applied Fluid Mechanics*, vol. 2, no. 2, pp. 29–34, 2012.

[45] I. L. Animasaun and A. O. Oyem, "Effect of variable viscosity, Dufour, Soret and thermal conductivity on free convective heat and mass transfer of non-Darcian flow past porous flat surface," *American Journal of Computational Mathematics*, vol. 4, no. 4, pp. 357–365, 2014.

[46] A. Raptis, "Flow of a micropolar fluid past a continuously moving plate by the presence of radiation," *International Journal of Heat and Mass Transfer*, vol. 41, no. 18, pp. 2865-2866, 1998.

[47] A. Raptis, "Radiation and viscoelastic flow," *International Communications in Heat and Mass Transfer*, vol. 26, no. 6, pp. 889–895, 1999.